





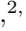

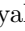
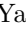



High-Fidelity Individual Addressing of Single Atoms in Quantum Registers at Three-Photon Laser Excitation of Rydberg States

N.N.Bezuglov ^{1,2} I.I.Beterov ^{2,3} A.Cinins ^{4,*} K.Miculis ^{4,5} V.M.Entin ² P.I.Betleni ^{2,3}
G.Suliman ^{2,3} V.V.Gromyko ² D.B.Tretyakov ^{2,3} E.A.Yakshina ^{2,3} and I.I.Ryabtsev ^{2,3}

¹*Saint-Petersburg State University, 199034 St.Petersburg, Russia*

²*Rzhanov Institute of Semiconductor Physics SB RAS, 630090 Novosibirsk, Russia*

³*Novosibirsk State University, Department of Physics, 630090 Novosibirsk, Russia*

⁴*Institute of Atomic Physics and Spectroscopy, Faculty of Science and Technology, University of Latvia, Jelgavas Street 3, LV-1004 Riga, Latvia*

⁵*National Research Nuclear University MEPhI, Moscow, 115409 Russia*

(Dated: November 12, 2024)

Precise individual addressing of single atoms in quantum registers formed by optical trap arrays is essential to achieve high-fidelity quantum gates in neutral-atom quantum computers and simulators. Two-qubit quantum gates are typically realized using coherent two-photon laser excitation of atoms to strongly interacting Rydberg states. However, two-photon excitation encounters challenges in individual addressing with tightly focused laser beams due to atom position uncertainty and the spatial inhomogeneity in both Rabi frequencies and light shifts. In this work, we theoretically demonstrate that the fidelity of individual addressing can be improved by employing coherent three-photon laser excitation of Rydberg states. For a specific example of $5s_{1/2} \xrightarrow{\Omega_1} 5p_{3/2} \xrightarrow{\Omega_2} 6s_{1/2} \xrightarrow{\Omega_3} np$ excitation in ^{87}Rb atoms, we find that upon strong laser coupling in the second step (Rabi frequency Ω_2) and moderate coupling in the first and third steps (Rabi frequencies Ω_1 and Ω_3), the three-photon Rabi frequency is given by $\Omega = \Omega_1\Omega_3/\Omega_2$. If the spatial distributions of $(\Omega_1\Omega_3)$ and Ω_2 are arranged to be identical, Ω becomes independent of atom position, even within very tightly focused laser beams. This approach dramatically improves individual addressing of Rydberg excitation for neighboring atoms in trap arrays compared to conventional two-photon excitation schemes. Our findings are crucial for large-scale quantum registers of neutral atoms, where distances between adjacent atoms should be minimized to ensure stronger Rydberg interactions and compact arrangement of atom arrays.

PACS numbers: 32.80.Ee, 32.70.Jz, 32.80.Rm, 03.67.Lx

Neutral-atom-based quantum computers and simulators represent a rapidly growing research field, which is close to practical realization [1–5]. The main advantage of this platform is its nearly unlimited potential for scalability to very large numbers of qubits, represented by single atoms trapped in optical dipole trap arrays [6]. Several recent studies have demonstrated quantum registers with thousands of qubits [7–9]. High-fidelity single-qubit gates in atomic arrays have been demonstrated both without individual addressing [10, 11] and with individual addressing [12, 13], though with a slight reduction in fidelity. Implementing two-qubit gates, which are essential for a universal quantum computer, poses a greater challenge. These gates rely on laser excitation to strongly interacting Rydberg states and on the associated Rydberg blockade effect [1–5, 14]. High-fidelity two-qubit gates using spatially homogeneous laser beams for Rydberg excitation have recently been demonstrated [15–22], with fidelities reaching 0.997 [22]. These fidelities are comparable to those achieved in superconducting [23] or ion [24] qubits, which, however, have not yet been scaled to thousands of qubits. Unfortunately, using tightly focused laser beams for individual addressing of single pairs of atoms in the array reduces two-qubit gate fidelities to around 0.95 [25]. This presents a significant obsta-

cle to building a universal quantum computer. Without individual addressing, coherent transport in atomic arrays partially resolves this issue by controlling inter-atomic interaction energy through adjustments in atom spacing [17]. However, this approach requires constant rearrangement of the atomic array for each quantum algorithm, which is technically challenging.

The primary challenge in achieving higher fidelity with neutral atoms is the finite atom temperature, typically in the microkelvin range for optical dipole trap experiments. While lower temperatures are possible through sideband Raman cooling [26], laser excitation to Rydberg states reheats the atoms to the microkelvin scale. Residual thermal atom motion introduces inhomogeneity in the Rabi frequency of Rydberg excitation when tightly focused laser beams are used, as the local laser field varies with atom position within the beam. In two-photon excitation schemes, spatially inhomogeneous light shifts that depend on atom position also induce decoherence in Rydberg excitation. To reduce inhomogeneity effects in two-photon excitation, less focused laser beams are required, which reduces single-qubit addressability and increases cross-talk with neighboring qubits. Mitigating the cross-talk requires increased spacing between adjacent atoms, yet in large-scale quantum registers, minimizing atom

distances is essential to ensure stronger Rydberg interactions and a compact atomic array layout.

In this paper, we theoretically demonstrate the potential for dramatically improving the fidelity of individual addressing and quantum gates by eliminating light shifts and inhomogeneity effects within the framework of three-photon excitation of Rydberg states. Several of our previous works have highlighted distinctive features of three-photon schemes. For instance, we have shown that both Doppler and recoil effects can be completely suppressed in the geometry of three laser beams with a zero sum of their wave vectors [27]. Figure 1(a) shows the three-photon excitation scheme $5s_{1/2} \rightarrow 5p_{3/2} \rightarrow 6s_{1/2} \rightarrow np$ in ^{87}Rb atoms, previously used in our experimental studies of Rydberg states [3, 28–33]. In our most recent work [33], we observed three-photon Rabi oscillations in the Rydberg excitation of a single ^{87}Rb atom in an optical dipole trap for the first time. To observe these Rabi oscillations, we applied a strong resonant radiation on the first and third steps, while the resonant radiations on the second step, while the resonant radiations on the first and third steps were set to moderate levels. Preliminary theoretical analysis had shown that a strong coupling in the second step induces ac Stark splitting of the intermediate levels $5P_{3/2}$ and $6S_{1/2}$, and introduces effective detunings on the intermediate transitions, ensuring coherence in the three-photon excitation.

To illustrate the key advantages of introducing the auxiliary intermediate $6s_{1/2}$ state, we examine the three-step ladder excitation of Fig. 1(a) with strong laser coupling in the second step and compare its properties to the two-photon excitation scheme $5s_{1/2} \rightarrow 6p_{3/2} \rightarrow ns_{1/2}$ of Fig. 1(b), which is commonly used in quantum information processing experiments with Rydberg atoms [15–17, 19, 20]. The corresponding two-photon linkage diagram is depicted in Fig. 1(c), where the laser Rabi frequencies $\Omega_{1,2}(r)$ are functions of the radial coordinate r of coaxial laser beams [see Eq. (7) below]. Far from single-photon resonance, $\delta_1 \gg \Omega_{1,2}$, the spatially inhomogeneous two-photon Rabi frequency $\Omega(r)$ and the two-photon detuning $\Delta(r)$ [see Fig. 1(c)] are given [34] by

$$\Omega = \Omega_1(r)\Omega_2(r)/(2\delta_1); \quad \Delta = [\Omega_2^2(r) - \Omega_1^2(r)]/(4\delta_1). \quad (1)$$

In further discussion of the three-photon scheme features, we denote states $5s_{1/2}, 5p_{3/2}, 6s_{1/2}, np$ in Fig. 1(a) as states $|1\rangle, |2\rangle, |3\rangle, |4\rangle$ respectively [see the corresponding linkage diagram in Fig. 1(e)]. For each intermediate single-photon transition $j = 1, 2, 3$ we denote the respective detunings as δ_j and the Rabi frequencies as $\Omega_j = d_j E_j / \hbar$. Here d_j are dipole moments of the single-photon transitions and E_j are electric-field amplitudes of the linearly polarized light fields. Due to the strong laser radiation ($\Omega_2 \gg \Omega_{1,3}$) driving the second excitation step, the corresponding strong ac Stark splitting of the intermediate levels $5P_{3/2}, 6S_{1/2}$ results in large effective detunings $\simeq \Omega_2/2$ [see Fig. 1(d)], rendering these levels

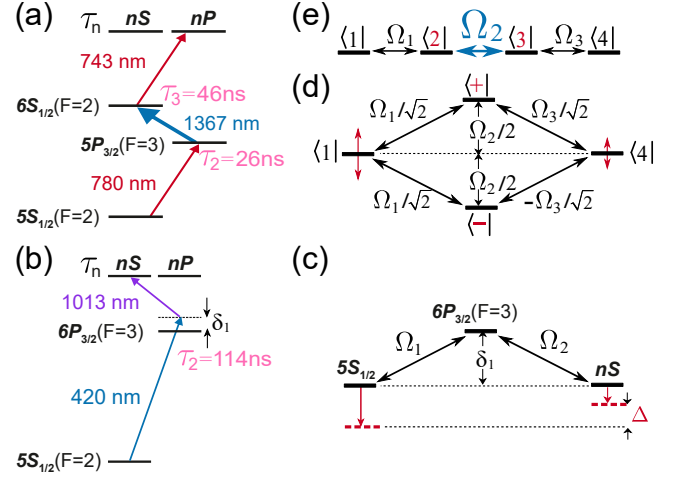


FIG. 1. (a) Three-photon [3, 28–33] and (b) two-photon [15–17, 19, 20] excitation schemes of Rydberg nP, nS states in ^{87}Rb atoms with the corresponding linkage diagrams (e,d), (c) in the rotating-wave approximation. The case of exact resonances [$\delta_{1,2,3} = 0$ in Eq. (3)] for all three lasers in frames (d,e) and two-photon resonance with single-photon detuning δ_1 in frame (c) are presented. All intermediate states, with lifetimes τ marked in pink, become virtual either due to the high intensity ($\Omega_2 \gg \Omega_{1,3}$) of the intermediate laser [frames (e,d)] or due to the large ($\delta_1 \gg \Omega_{1,2}$) single-photon detuning [frame (c)]. Both the ground $5S_{1/2}$ and the Rydberg nS states in frame (c) experience different ac Stark shifts (marked in red), leading to a spatially inhomogeneous two-photon detuning $\Delta(r)$ (1). In frame (e), a very strong laser coupling between the intermediate states $|2\rangle, |3\rangle$ transforms them into virtual $|\pm\rangle = (|2\rangle \pm |3\rangle)/\sqrt{2}$ states as shown in frame (d). Due to the resulting mirror-symmetric atomic states configuration, each of the states $|1\rangle, |4\rangle$ experiences two identical ac Stark shifts (indicated by the red vertical arrows) with opposite signs, which makes the aggregate light shifts of states $|1\rangle, |4\rangle$ vanish for any choice of Rabi frequencies Ω_1, Ω_3 .

nearly unpopulated. Therefore, as a reasonable approximation [35], instead of using the density matrix formalism to describe the temporal dynamics of a four-level system with radiatively decaying intermediate states, we can work in terms of the probability amplitudes $C_j(t)$ of the levels satisfying the reduced Schrödinger equation

$$\begin{aligned} i\dot{C}_1 &= \Omega_1 C_2 e^{i\delta_1 t} / 2, \\ i\dot{C}_2 &= (-iC_2/\tau_2 + \Omega_1 C_1 e^{-i\delta_1 t} + \Omega_2 C_3 e^{i\delta_2 t}) / 2, \\ i\dot{C}_3 &= (-iC_3/\tau_3 + \Omega_2 C_2 e^{-i\delta_2 t} + \Omega_3 C_4 e^{i\delta_3 t}) / 2, \\ i\dot{C}_4 &= (-iC_4/\tau_4 + \Omega_3 C_3 e^{-i\delta_3 t}) / 2, \end{aligned} \quad (2)$$

written in the rotating wave approximation. The radiative decays of both virtual intermediate and long-lived Rydberg states with radiative lifetimes τ_j are taken into account in Eq. (2) by adding relaxation rate constants $1/\tau_j$ to the imaginary parts of the corresponding state energies [34–36].

The strong coupling of the intermediate states $|2\rangle, |3\rangle$,

accompanied by their large splitting $\approx \Omega_2$, much larger than all other laser Rabi frequencies Ω_j and detunings δ_j , allows an important simplification. Namely, for the amplitudes $C_{2,3}$ of the intermediate states one can apply the adiabatic elimination procedure [35, 37, 38], according to which the derivatives $\dot{C}_2, \dot{C}_3 \approx 0$, since their values are expected to be much smaller than the other terms. As a result, Eqs. (2) are reduced to equations

$$\begin{aligned} i\dot{C}_1 &\approx \left(-i\bar{\gamma}_1 C_1 - \Omega \cdot C_4 e^{i\bar{\delta}t}\right) / 2, \\ i\dot{C}_4 &\approx \left(-i\bar{\gamma}_4 C_4 - \Omega \cdot C_1 e^{-i\bar{\delta}t}\right) / 2 \end{aligned} \quad (3)$$

for an effective two-level system, involving only amplitudes C_1, C_4 . The three-photon detuning $\bar{\delta}$, reduced Rabi frequency Ω and relaxation constants $\bar{\gamma}_{1,4}$ have the following form:

$$\begin{aligned} \bar{\delta} &= \delta_1 + \delta_2 + \delta_3; \quad \Omega = \Omega_1 \Omega_3 / \Omega_2; \quad \bar{\gamma}_1 = \bar{\gamma} \cdot \Omega_1^2 / \Omega_2^2; \\ \bar{\gamma}_4 &= \bar{\gamma} \cdot \Omega_3^2 / \Omega_2^2 + 1 / \tau_4; \quad \bar{\gamma} = (1 / \tau_2 + 1 / \tau_3) / 2. \end{aligned} \quad (4)$$

Importantly, when $\tau_2 \neq \tau_3$ the conventional adiabatic elimination procedure ($\dot{C}_{2,3} \rightarrow 0$) requires some corrections [38], which we have taken into account for the rate constants $\bar{\gamma}_{1,4}$ in Eq. (4).

Since we are concerned with the case $\Omega_2 \gg \Omega_{1,3}, 1 / \tau_j, |\bar{\delta}|$, Eq. (4) gives us an important set of inequalities:

$$\bar{\gamma}_j = \frac{\bar{\gamma}}{\Omega_2} \frac{\Omega_j}{\Omega_{k \neq j}} \Omega \ll \Omega; \quad j, k = 1, 4. \quad (5)$$

This significantly simplifies the formulaic representations of Eq. (3) solutions along with the corresponding Rydberg states population $n_4 = |C_4|^2$, which under the initial conditions $C_1(0) = 1, C_4(0) = 0$ acquires a compact form

$$\begin{aligned} n_4 &\approx \frac{\Omega^2}{2\bar{\Omega}^2} [1 - \cos(\bar{\Omega} \cdot t)] e^{-\Gamma t / 2}; \\ \bar{\Omega} &= \sqrt{\Omega^2 + \bar{\delta}^2}; \quad \Gamma = \frac{\Omega_1^2 + \Omega_3^2}{\Omega_2^2} \bar{\gamma} + \frac{1}{\tau_4}, \end{aligned} \quad (6)$$

describing slowly fading coherent three-photon Rabi oscillations at frequency $\bar{\Omega}$. The first term in the decay constant Γ of Eq. (6) accounts for decoherence due to a small partial population of the short-lived intermediate states $|2\rangle, |3\rangle$, while the second term is due to the long lifetime of the Rydberg state $|4\rangle$. In the following discussion we mainly focus on the case of resonant lasers with $\delta_{1,2,3} = 0$, i.e. when the three-photon detuning $\bar{\delta} = 0$ and $\bar{\Omega} = \Omega$. The one exception is the spectral profiles in Fig. 2(a), obtained by varying δ_3 around zero.

Noteworthy, the three-photon Rabi frequency (4) takes a form similar to the two-photon case (1), with the Rabi frequency $\Omega_2/2$ taking the role of the single-photon detuning δ_1 in Fig. 1(c). The large Ω_2 in Fig. 1(e) forms two adiabatic states $|\pm\rangle = (|2\rangle \pm |3\rangle) / \sqrt{2}$, thus virtually

converting the three-photon excitation into a double two-photon scheme depicted in Fig. 1(d) by inducing light shifts $\pm \Omega_2/2$ with two fundamentally new properties:

First, if we arrange the spatial distributions of $(\Omega_1 \Omega_3)$ and Ω_2 to be identical, then Ω becomes independent of the atom position, even with tightly focused laser beams. This enables a significantly improved individual addressing of Rydberg excitations for adjacent atoms in trap arrays, compared to two-photon excitation schemes. In addition, tight focusing strongly reduces the total laser power required to excite Rydberg atoms in large-scale quantum registers of neutral atoms.

Second, the essential trait of the reduced Eq. (3) is the total elimination of ac Stark shifts $\Delta_{j=1,4}$ for both the ground and Rydberg states. Because of the mirror-image arrangement of the virtual levels $|\pm\rangle$ in the linkage diagram, associated with Eq. (2) and shown in Fig. 1(d), they cause two partial identical but opposite optical shifts $\Delta_{j\pm}$ of each j -state, making the overall shift Δ_j zero at arbitrary laser intensities. As a result, the three-photon detuning $\Delta = \Delta_4 - \Delta_1$ turns out to be insensitive to any spatial inhomogeneities of the laser fields. Therefore, even in tightly focused laser beams with radically different Ω_1 and Ω_3 values, the spatially inhomogeneous light shifts will be absent. The latter can significantly increase the coherence and fidelity of Rydberg quantum gates.

The above simple analysis highlights the main advantages of using three-photon laser excitation of Rydberg states for both individual addressing and light-shift suppression. Next we demonstrate how these advantages are manifested in accurate numerical calculations of light shifts and Rabi oscillations.

A full rigorous theoretical analysis must deal with the density matrix formalism and the optical Bloch equations [35, 37], traditionally used to describe atom-light interaction processes, and taking into account the real hyperfine and Zeeman structures of all states involved in the interaction. In our previous works [39, 40] we developed an efficient algorithm based on the split operator technique [41, 42], which provides robust symplectic [43, 44] numerical simulations of laser excitation of alkali metal atoms. Details of the algorithm specific parameters as applied to Rb and Na atoms can be found in [40, 45].

Figure 2 presents results of our numerical simulations of the spectra profiles for the cases of (a) three-photon and (b) two-photon Rydberg states excitation in ^{87}Rb atoms for a fixed interaction time of $0.125 \mu\text{s}$. The radiative lifetimes of the Rydberg states at $T=300 \text{ K}$ are $\tau(70p_{3/2}) = 190 \mu\text{s}$ and $\tau(70s_{1/2}) = 152 \mu\text{s}$, respectively. The lifetimes of intermediate states are schematically shown in Fig. 1. The strong coupling of intermediate states in case (a) and the large single-photon detuning δ_1 in case (b) make all the intermediate states virtual. Our numerical simulations clearly demonstrate in Fig. 2(a) the absence of ac Stark shifts for arbitrary values of the

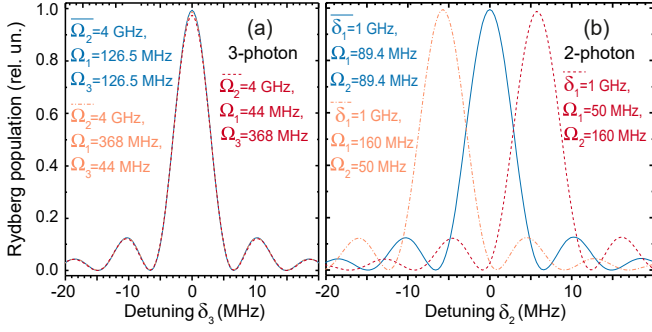


FIG. 2. (a) Numerically obtained spectra of the three-photon excitation $5s_{1/2} \rightarrow 5p_{3/2} \rightarrow 6s_{1/2} \rightarrow 70p_{3/2}$ [see Fig. 1(a)] in ^{87}Rb atoms for an interaction time of $0.125 \mu\text{s}$ at a high second-step laser Rabi frequency $\Omega_2/(2\pi) = 4 \text{ GHz}$ and various ratios between the modest first-step Ω_1 and third-step Ω_3 frequencies, providing a fixed three-photon Rabi frequency $\Omega/(2\pi) = 4 \text{ MHz}$. No light shift is observed for any combination of $\Omega_{1,3}$. (b) The same for the two-photon excitation $5s_{1/2} \rightarrow 6p_{3/2} \rightarrow 70s_{1/2}$ [see Fig. 1(b)] in ^{87}Rb atoms for an interaction time of $0.125 \mu\text{s}$ at first-step detuning $\delta_1/(2\pi) = 1 \text{ GHz}$ and various ratios between the first-step Ω_1 and second-step Ω_2 laser frequencies, resulting in the same two-photon Rabi frequency $\Omega/(2\pi) = 4 \text{ MHz}$. A strong two-photon detuning Δ is observed when $\Omega_1 \neq \Omega_2$ in agreement with Eq. (1). All spectra in both frames (a), (b) refer to the case of wide laser beams.

laser Rabi frequencies $\Omega_{1,3}$. In contrast, Fig. 2(b) demonstrates a strong dependence of the two-photon resonance position on the imbalance parameter Ω_2/Ω_1 between the Rabi frequencies. Therefore, spatial inhomogeneity or intensity fluctuations of the laser radiations would strongly affect two-photon excitation, while three-photon excitation is robust against these factors.

The ability to achieve a spatially homogeneous Rabi frequency Ω (4) with a special laser beam arrangement is the most distinctive feature of the three-photon scheme. This configuration enables highly coherent excitation of Rydberg states even in very tightly focused beams, as illustrated in Figs. 3, 4. In cylindrical coordinates r, φ , the coaxial laser beams have Gaussian Rabi frequency profiles with respect to the transverse radial coordinate

$$\Omega_j(r) = \Omega_j e^{-r^2/w_j^2}; \quad \Omega_j \equiv \Omega_j(r=0). \quad (7)$$

The parameters w_j ($j = 1 - 3$) represent the $1/e^2$ laser focal spot radii, usually measured in experiments. The following relationship

$$w_1 = w_3 = \sqrt{2}w_2 \equiv w; \Rightarrow \Omega(r) = \frac{\Omega_1(r=0)\Omega_3(r=0)}{\Omega_2(r=0)} \quad (8)$$

between laser spots guarantees the constancy of the three-photon Rabi oscillation frequency for any spatial position of the atom. This is a very important finding, since the atom in an optical dipole trap is not localized point-wise. Instead, the atom density has some

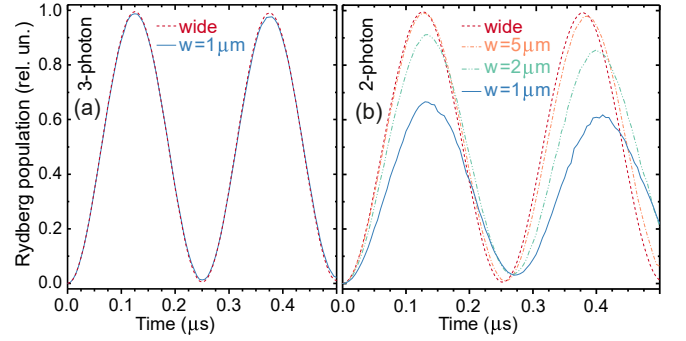


FIG. 3. (a) Rabi oscillations simulations for three-photon excitation $5s_{1/2} \rightarrow 5p_{3/2} \rightarrow 6s_{1/2} \rightarrow 70p_{3/2}$ in ^{87}Rb atoms with strong second-step laser coupling $\Omega_2/(2\pi) = 4 \text{ GHz}$ and moderate first and third-step Rabi frequencies $\Omega_1/(2\pi) = \Omega_3/(2\pi) = 126.5 \text{ MHz}$. The dashed red curve corresponds to spatially uniform (wide) laser beams, while the solid blue curve describes the spatially averaged oscillations $\langle n_4 \rangle$ at $a = 1 \mu\text{m}$ and $w = 1 \mu\text{m}$ for the radii of the atomic a (9) and the laser w (8) spots, respectively. Spatial variation of Rabi frequencies $\Omega_j(r)$ does not noticeably affect contrast of the curve. (b) The same for the two-photon excitation $5s_{1/2} \rightarrow 6p_{3/2} \rightarrow 70s_{1/2}$ in ^{87}Rb atoms for single-photon detuning $\delta_1/(2\pi) = 1 \text{ GHz}$ and first- and second-step Rabi frequencies $\Omega_1/(2\pi) = 160 \text{ MHz}$, $\Omega_2/(2\pi) = 50 \text{ MHz}$, respectively, as used in [16]. Laser spot radius varies from a very large value (wide beams) to $w = 5, 2, 1 \mu\text{m}$. The spatial variations of Rabi frequencies $\Omega_{1,2}(r)$ strongly reduce the contrast in tightly focused laser beams.

azimuthally invariant radial distribution $\rho(r)$, reasonably well approximated by a normalized Gaussian function [34]

$$\rho(r) = \frac{2}{\pi a^2} e^{-2r^2/a^2}. \quad (9)$$

The parameter a is the atom spot radius for the probability level $1/e^2$. It is determined by the waist radius w_0 of the optical dipole trap, atom temperature T , and trap depth U_0 , and can be estimated as $a \sim w_0 \sqrt{k_B T/U_0}$ [34], where k_B is the Boltzmann constant. For the typical trap depth $\sim 1 \text{ mK}$ and atom temperature $\sim 10 \mu\text{K}$, one has $a \sim w_0/10$.

The Rabi oscillations observed in an experiment represent the average population $\langle n_4 \rangle$ (6) over spatial coordinates r, φ , with the weight function $\rho(r)$ (9). Figure 3 presents numerically calculated Rabi oscillations of (a) three-photon and (b) two-photon excitation in ^{87}Rb atoms. The data in frame (a) are calculated for a large laser Rabi frequency in the second step, and equal moderate Rabi frequencies applied to the first and third excitation steps. The two-photon oscillation curves in frame (b) were calculated using the single-photon detuning and the first- and second-step Rabi frequencies values from [16]. The dashed red curves in both frames of Fig. 3 correspond to spatially uniform (wide) laser beams. Both curves have the same three- and two-photon Rabi os-

illation frequencies of 4 MHz and identical oscillation contrasts. The other curves in Fig. 3 show how the spatially averaged Rabi oscillations depend on different relationships between the uncertainty of the atomic position and the laser spot size. The curves indicate a completely different character of the destructive influence of spatial inhomogeneities of laser fields on the oscillation contrast for two- and three-step schemes. In a more detailed discussion below, we will obtain a formulaic description for the effects of spatial variation in laser intensities.

For our three-photon excitation, the radial dependence of the Rydberg state population (6) arises only due to variation in the effective relaxation constant Γ included in the amplitude part of Eq. (6):

$$\Gamma(r) = \frac{\Omega_1^2(0) + \Omega_3^2(0)}{2\Omega_2^2(0)} \left(\frac{1}{\tau_2} + \frac{1}{\tau_3} \right) e^{2r^2/w^2} + \frac{1}{\tau_4}, \quad (10)$$

which is a consequence of the relation (8) for laser focal spots. Importantly, the population averaging procedure affects only the relaxation factor, leaving the oscillatory part in Eq. (6) unchanged.

The main practically important parameter of Rabi oscillations, which directly defines the maximum achievable fidelity of Rydberg quantum gates, is the amplitude A_1 of the first oscillation peak in Eq. (6). The latter occurs at time $t = \pi/\Omega$. For a given spatial point with coordinate r and for $\Omega \gg \Gamma(r)$, the peak height is expressed as

$$n_4(r)_{max} = e^{-\Gamma(r)t/2} \approx 1 - \pi\Gamma(r)/(2\Omega). \quad (11)$$

Averaging of Eq. (11) over cylindrical spacial coordinates r, φ with the weight function (9) yields

$$A_1 \equiv \langle n_4(t) \rangle_{max} \approx 1 - \frac{\pi}{2\Omega} \left[\frac{\Gamma(0)\xi^2}{\xi^2 - 1} - \frac{\tau_4^{-1}}{\xi^2 - 1} \right], \quad (12)$$

where the ‘‘coverage’’ parameter $\xi = w/a$ shows how much the Rydberg laser spot exceeds (‘‘covers’’) the atom spot.

Figure 4(a) shows the numerically identified (circles) and analytically calculated using Eq. (12) (blue curve) dependences of the spatially averaged amplitude A_1 on the ratio w/a for three-photon excitation in ^{87}Rb atoms, with the same parameters as in Fig. 3(a). A fairly good agreement between the analytical model and numerical simulation is observed for $w/a \geq 2$. We also see a slow decline in A_1 in the interval $1 \leq w/a \leq 2$, where the amplitude remains close to its maximum possible value of 0.9957. Moreover, even for $w/a = 1$ the value of A_1 drops to only slightly lower value of 0.9877. This change in A_1 is almost imperceptible in the Rabi oscillations shown in Fig. 3(a). Our simulations confirm the validity of the above proposal for high precision addressing with three-photon Rydberg excitation, and show that it should be experimentally feasible.

The obtained results open up prospects for an experimental solution to the problem of local addressing in

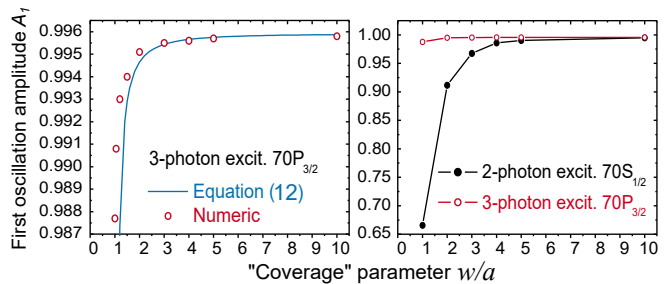


FIG. 4. (a) Numerically (circles) and analytically (blue curve) obtained spatially averaged amplitude A_1 of the first Rabi oscillation at three-photon excitation $5s_{1/2} \rightarrow 5p_{3/2} \rightarrow 6s_{1/2} \rightarrow 70p_{3/2}$ in ^{87}Rb atoms, for the same parameters as in Fig. 3(a). The circles and the curve demonstrate the dependence of amplitude A_1 on the ‘‘coverage’’ parameter w/a . Fairly good agreement is observed for $w/a \geq 2$. (b) Comparison of numerically calculated spatially averaged amplitude A_1 for three-photon excitation corresponding to frame (a) and two-photon excitation $5s_{1/2} \rightarrow 6p_{3/2} \rightarrow 70s_{1/2}$ in ^{87}Rb atoms, for the same parameters as in Fig. 3(b). Under three-photon excitation, contrast of the first peak remains virtually unchanged even in fairly narrow laser beams with a coverage parameter of $w/a = 2$. In contrast, the two-photon oscillations exhibit a significant drop of A_1 amplitude in moderately narrow beams with $w/a \leq 5$.

atomic arrays. A typical experiment with single atoms in quantum registers assumes the values of atomic and laser spots to be $a \sim 1 \mu\text{m}$ and $w \sim 2-3 \mu\text{m}$, respectively, and the distance between neighboring atoms of $\sim 5 \mu\text{m}$. At the Rabi frequencies Ω_j used in Fig. 4(a), the calculated amplitude A_1 of the first oscillation is 0.9951 at $w/a = 2$. The significant exponential drop of Ω_j in Eq. (7) strongly suppresses the Rydberg excitation of the neighboring atoms: the calculations yield a negligible value of $\sim 10^{-5} - 10^{-6}$ for their Rydberg state populations.

The above observation is not the case for two-photon excitation. Figure 4(b) shows the comparison of numerically calculated spatially-averaged amplitudes A_1 of the first Rabi oscillation at three-photon excitation and two-photon excitation in ^{87}Rb atoms for the same parameters as in Fig. 3(b). While the three-photon amplitude A_1 in Fig. 4(b) is almost independent of the change in w/a , the two-photon amplitude decreases significantly starting from $w/a = 5$. At $w/a = 1$ it drops to 0.662 compared to 0.9949 for $w/a = 10$ and 0.9956 for wide laser beams. At $w/a = 2$ the two-photon amplitude A_1 takes the value 0.912, which is no longer suitable for quantum gates. Therefore, precise individual addressing cannot be implemented with two-photon Rydberg excitation in atom arrays with spacing of $\sim 5 \mu\text{m}$. To avoid crosstalk problems, the distance should be increased to at least $\sim 20 \mu\text{m}$, while using wide laser beams with $w/a \sim 10$. This prevents implementation of large-scale quantum registers with neutral atoms, where the smallest possible distance between adjacent atoms is necessary to ensure strong

interaction of Rydberg states and compact packing of atomic arrays.

In conclusion, we have shown theoretically that high-fidelity individual addressing of single atoms and the mitigation of crosstalk in optical dipole trap arrays can be achieved using three-photon laser excitation of Rydberg states, provided that strong laser radiation in the second step induces a dominant ac Stark splitting of the two intermediate states. Moreover, this excitation method suppresses the light shift of the three-photon resonance, even in cases of arbitrary imbalance between the Rabi frequencies in the first and third steps. Thus, three-photon Rydberg excitation offers a substantial advantage over the commonly used two-photon excitation, in which individual addressing and light-shift suppression are challenging to implement experimentally.

Authors N.N.B., I.I.B., and I.I.R. acknowledge the support of the grant No. 23-12-00067 (<https://rscf.ru/project/23-12-00067/>) by the Russian Science Foundation. Author A.C. acknowledges the support of Latvian Council of Science project No. lzp-2023/1-0199.

* arturs.cinins@lu.lv

- [1] M. Saffman, T. G. Walker, and K. Mølmer, Quantum information with rydberg atoms, *Rev. Mod. Phys.* **82**, 2313 (2010).
- [2] M. Saffman, Quantum computing with atomic qubits and rydberg interactions: progress and challenges, *Journal of Physics B: Atomic, Molecular and Optical Physics* **49**, 202001 (2016).
- [3] I. I. Ryabtsev, I. I. Beterov, D. B. Tret'yakov, V. M. Entin, and E. A. Yakshina, Spectroscopy of cold rubidium rydberg atoms for applications in quantum information, *Physics-Uspekhi* **59**, 196–208 (2016).
- [4] L. Henriët, L. Beguin, A. Signoles, T. Lahaye, A. Browaeys, G.-O. Reymond, and C. Jurczak, Quantum computing with neutral atoms, *Quantum* **4**, 327 (2020).
- [5] X.-F. Shi, Quantum logic and entanglement by neutral rydberg atoms: methods and fidelity, *Quantum Science and Technology* **7**, 023002 (2022).
- [6] D. Barredo, S. de Léséleuc, V. Lienhard, T. Lahaye, and A. Browaeys, An atom-by-atom assembler of defect-free arbitrary two-dimensional atomic arrays, *Science* **354**, 1021 (2016).
- [7] L. Pause, L. Sturm, M. Mittenbühler, S. Amann, T. Preuschoff, D. Schäffner, M. Schlosser, and G. Birkl, Supercharged two-dimensional tweezer array with more than 1000 atomic qubits, *Optica* **11**, 222 (2024).
- [8] G. Pichard, D. Lim, E. Bloch, J. Vaneeccloo, L. Bourachot, G.-J. Both, G. Mériaux, S. Dutartre, R. Hosten, J. Paris, B. Ximenez, A. Signoles, A. Browaeys, T. Lahaye, and D. Dreon, Rearrangement of individual atoms in a 2000-site optical-tweezer array at cryogenic temperatures, *Phys. Rev. Appl.* **22**, 024073 (2024).
- [9] H. J. Manetsch, G. Nomura, E. Bataille, K. H. Leung, X. Lv, and M. Endres, A tweezer array with 6100 highly coherent atomic qubits (2024), arXiv:2403.12021 [quant-ph].
- [10] C. Sheng, X. He, P. Xu, R. Guo, K. Wang, Z. Xiong, M. Liu, J. Wang, and M. Zhan, High-fidelity single-qubit gates on neutral atoms in a two-dimensional magic-intensity optical dipole trap array, *Phys. Rev. Lett.* **121**, 240501 (2018).
- [11] B. Nikolov, E. Diamond-Hitchcock, J. Bass, N. L. R. Spong, and J. D. Pritchard, Randomized benchmarking using nondestructive readout in a two-dimensional atom array, *Phys. Rev. Lett.* **131**, 030602 (2023).
- [12] S. Ma, G. Liu, P. Peng, B. Zhang, S. Jandura, J. Claes, A. P. Burgers, G. Pupillo, S. Puri, and J. D. Thompson, High-fidelity gates and mid-circuit erasure conversion in an atomic qubit, *Nature* **622**, 279 (2023).
- [13] A. Jenkins, J. W. Lis, A. Senoo, W. F. McGrew, and A. M. Kaufman, Ytterbium nuclear-spin qubits in an optical tweezer array, *Phys. Rev. X* **12**, 021027 (2022).
- [14] M. D. Lukin, M. Fleischhauer, R. Cote, L. M. Duan, D. Jaksch, J. I. Cirac, and P. Zoller, Dipole blockade and quantum information processing in mesoscopic atomic ensembles, *Phys. Rev. Lett.* **87**, 037901 (2001).
- [15] H. Levine, A. Keesling, A. Omran, H. Bernien, S. Schwartz, A. S. Zibrov, M. Endres, M. Greiner, V. Vuletić, and M. D. Lukin, High-fidelity control and entanglement of rydberg-atom qubits, *Phys. Rev. Lett.* **121**, 123603 (2018).
- [16] H. Levine, A. Keesling, G. Semeghini, A. Omran, T. T. Wang, S. Ebadi, H. Bernien, M. Greiner, V. Vuletić, H. Pichler, and M. D. Lukin, Parallel implementation of high-fidelity multiqubit gates with neutral atoms, *Phys. Rev. Lett.* **123**, 170503 (2019).
- [17] S. Ebadi, T. T. Wang, H. Levine, A. Keesling, G. Semeghini, A. Omran, D. Bluvstein, R. Samajdar, H. Pichler, W. W. Ho, S. Choi, S. Sachdev, M. Greiner, V. Vuletić, and M. D. Lukin, Quantum phases of matter on a 256-atom programmable quantum simulator, *Nature* **595**, 227 (2021).
- [18] Z. Fu, P. Xu, Y. Sun, Y.-Y. Liu, X.-D. He, X. Li, M. Liu, R.-B. Li, J. Wang, L. Liu, and M.-S. Zhan, High-fidelity entanglement of neutral atoms via a rydberg-mediated single-modulated-pulse controlled-phase gate, *Phys. Rev. A* **105**, 042430 (2022).
- [19] S. J. Evered, D. Bluvstein, M. Kalinowski, S. Ebadi, T. Manovitz, H. Zhou, S. H. Li, A. A. Geim, T. T. Wang, N. Maskara, H. Levine, G. Semeghini, M. Greiner, V. Vuletić, and M. D. Lukin, High-fidelity parallel entangling gates on a neutral-atom quantum computer, *Nature* **622**, 268 (2023).
- [20] D. Bluvstein, S. J. Evered, A. A. Geim, S. H. Li, H. Zhou, T. Manovitz, S. Ebadi, M. Cain, M. Kalinowski, D. Hangleiter, J. P. Bonilla Ataides, N. Maskara, I. Cong, X. Gao, P. Sales Rodriguez, T. Karolyshyn, G. Semeghini, M. J. Gullans, M. Greiner, V. Vuletić, and M. D. Lukin, Logical quantum processor based on reconfigurable atom arrays, *Nature* **626**, 58 (2024).
- [21] A. G. Radnaev, W. C. Chung, D. C. Cole, D. Mason, T. G. Ballance, M. J. Bedalov, D. A. Belknap, M. R. Berman, M. Blakely, I. L. Bloomfield, P. D. Buttler, C. Campbell, A. Chopinaud, E. Copenhaver, M. K. Dawes, S. Y. Eubanks, A. J. Friss, D. M. Garcia, J. Gilbert, M. Gillette, P. Goiporia, P. Gokhale, J. Goldwin, D. Goodwin, T. M. Graham, C. Guttormsson, G. T. Hickman, L. Hurtle, M. Iliev, E. B. Jones, R. A. Jones,

- K. W. Kuper, T. B. Lewis, M. T. Lichtman, F. Majdemeimouri, J. J. Mason, J. K. McMaster, J. A. Miles, P. T. Mitchell, J. D. Murphree, N. A. Neff-Mallon, T. Oh, V. Omole, C. P. Simon, N. Pederson, M. A. Perlin, A. Reiter, R. Rines, P. Romlow, A. M. Scott, D. Stiefvater, J. R. Tanner, A. K. Tucker, I. V. Vinogradov, M. L. Warter, M. Yeo, M. Saffman, and T. W. Noel, A universal neutral-atom quantum computer with individual optical addressing and non-destructive readout (2024), arXiv:2408.08288 [quant-ph].
- [22] R. B.-S. Tsai, X. Sun, A. L. Shaw, R. Finkelstein, and M. Endres, Benchmarking and linear response modeling of high-fidelity rydberg gates (2024), arXiv:2407.20184 [quant-ph].
- [23] H.-L. Huang, D. Wu, D. Fan, and X. Zhu, Superconducting quantum computing: a review, *Science China Information Sciences* **63**, 180501 (2020).
- [24] C. D. Bruzewicz, J. Chiaverini, R. McConnell, and J. M. Sage, Trapped-ion quantum computing: Progress and challenges, *Applied Physics Reviews* **6**, 021314 (2019).
- [25] T. M. Graham, Y. Song, J. Scott, C. Poole, L. Phuttitarn, K. Jooya, P. Eichler, X. Jiang, A. Marra, B. Grinkemeyer, M. Kwon, M. Ebert, J. Cherek, M. T. Lichtman, M. Gillette, J. Gilbert, D. Bowman, T. Ballance, C. Campbell, E. D. Dahl, O. Crawford, N. S. Blunt, B. Rogers, T. Noel, and M. Saffman, Multi-qubit entanglement and algorithms on a neutral-atom quantum computer, *Nature* **604**, 457 (2022).
- [26] Z. Tian, H. Chang, X. Lv, M. Yang, Z. Wang, P. Yang, P. Zhang, G. Li, and T. Zhang, Resolved raman sideband cooling of a single optically trapped cesium atom, *Opt. Lett.* **49**, 542 (2024).
- [27] I. I. Ryabtsev, I. I. Beterov, D. B. Tretyakov, V. M. Entin, and E. A. Yakshina, Doppler- and recoil-free laser excitation of rydberg states via three-photon transitions, *Phys. Rev. A* **84**, 053409 (2011).
- [28] V. M. Entin, E. A. Yakshina, D. B. Tretyakov, I. I. Beterov, and I. I. Ryabtsev, Spectroscopy of the three-photon laser excitation of cold rubidium rydberg atoms in a magneto-optical trap, *Journal of Experimental and Theoretical Physics* **116**, 721 (2013).
- [29] E. Yakshina, D. Tretyakov, V. Entin, I. Beterov, and I. Ryabtsev, Three-photon laser excitation of mesoscopic ensembles of cold rubidium rydberg atoms, *Quantum Electronics* **48**, 886 (2018).
- [30] E. A. Yakshina, D. B. Tretyakov, V. M. Entin, I. I. Beterov, and I. I. Ryabtsev, Observation of the dipole blockade effect in detecting rydberg atoms by the selective field ionization method, *Journal of Experimental and Theoretical Physics* **130**, 170 (2020).
- [31] D. Tretyakov, V. Entin, E. Yakshina, I. Beterov, and I. Ryabtsev, Dynamics of three-photon laser excitation of mesoscopic ensembles of cold rubidium atoms to rydberg states, *Quantum Electronics* **52**, 513 (2022).
- [32] I. I. Beterov, E. A. Yakshina, D. B. Tretyakov, N. V. Al'yanova, D. A. Skvortsova, G. Suliman, T. R. Zagirov, V. M. Entin, and I. I. Ryabtsev, Three-photon laser excitation of single rydberg rubidium atoms in an optical dipole trap, *Journal of Experimental and Theoretical Physics* **137**, 246 (2023).
- [33] I. I. Beterov, E. A. Yakshina, G. Suliman, P. I. Betleni, A. A. Prilutskaya, D. A. Skvortsova, T. R. Zagirov, D. B. Tretyakov, V. M. Entin, N. N. Bezuglov, and I. I. Ryabtsev, Rabi oscillations at three-photon laser excitation of a single rubidium rydberg atom in an optical dipole trap, *Zh. Eksp. Teor. Fiz.* **166**, 535 (2024), [English translation at arXiv: <https://arxiv.org/abs/2410.01703>].
- [34] R. Grimm, M. Weidemüller, and Y. B. Ovchinnikov, Optical dipole traps for neutral atoms, in *Advances In Atomic, Molecular, and Optical Physics* (Elsevier, 2000) p. 95–170.
- [35] B. Shore, *Manipulating Quantum Structures Using Laser Pulses* (Cambridge University Press, 2009).
- [36] C. N. Cohen-Tannoudji, Nobel lecture: Manipulating atoms with photons, *Rev. Mod. Phys.* **70**, 707 (1998).
- [37] S. Stenholm, *Foundations of Laser Spectroscopy*, Dover Books on Physics (Dover Publications, 2012).
- [38] N. Macrì, L. Giannelli, E. Paladino, and G. Falci, Coarse-grained effective hamiltonian via the magnus expansion for a three-level system, *Entropy* **25**, 10.3390/e25020234 (2023).
- [39] T. Kirova, A. Cinins, D. K. Efimov, M. Bruvelis, K. Miculis, N. N. Bezuglov, M. Auzinsh, I. I. Ryabtsev, and A. Ekers, Hyperfine interaction in the autler-townes effect: The formation of bright, dark, and chameleon states, *Phys. Rev. A* **96**, 043421 (2017).
- [40] A. Cinins, D. K. Efimov, M. Bruvelis, K. Miculis, T. Kirova, N. N. Bezuglov, I. I. Ryabtsev, M. Auzinsh, and A. Ekers, Hyperfine interaction in the autler-townes effect: Control of two-photon selection rules in the morris-shore basis, *Phys. Rev. A* **109**, 063116 (2024).
- [41] A. K. Kazansky, N. N. Bezuglov, A. F. Molisch, F. Fuso, and M. Allegrini, Direct numerical method to solve radiation trapping problems with a doppler-broadening mechanism for partial frequency redistribution, *Phys. Rev. A* **64**, 022719 (2001).
- [42] D. K. Efimov, N. N. Bezuglov, A. N. Klyucharev, Y. N. Gnedin, K. Miculis, and A. Ekers, Analysis of light-induced diffusion ionization of a three-dimensional hydrogen atom based on the floquet technique and split-operator method, *Optics and Spectroscopy* **117**, 8 (2014).
- [43] E. Hairer, G. Wanner, and C. Lubich, *Geometric Numerical Integration: Structure-Preserving Algorithms for Ordinary Differential Equations* (Springer Berlin Heidelberg, Berlin, Heidelberg, 2006).
- [44] E. Hairer, C. Lubich, and G. Wanner, Geometric numerical integration illustrated by the störmer–verlet method, *Acta Numerica* **12**, 399–450 (2003).
- [45] I. Sydoryk, N. N. Bezuglov, I. I. Beterov, K. Miculis, E. Saks, A. Janovs, P. Spels, and A. Ekers, Broadening and intensity redistribution in the Na(3p) hyperfine excitation spectra due to optical pumping in the weak excitation limit, *Phys. Rev. A* **77**, 042511 (2008).